J Mater Sci: Mater Electron (2021) 32:11969–11977

Dielectric phase transition and ferroelectric properties of neodymium-doped $BaBi_4Ti_4O_{15}$ layered ceramics

Triloki Rana[1], J. P. Sharma[1,*], Bibek Kumar Sonu[2], and B. Parija[3]

[1] University Department of Physics, Dr. Shyama Prasad Mukherjee University, Ranchi, India
[2] Department of Physics, BIT, Mesra, Ranchi, India
[3] Department of Physics, Government Autonomous College, Rourkela, Odisha, India

Received: 4 December 2020
Accepted: 23 March 2021
Published online: 8 April 2021

ABSTRACT

The dielectric and ferroelectric properties of $Ba_{1-(3/2)x}Nd_xBi_4Ti_4O_{15}$ (BNBT) ceramics prepared by using the solid-state reaction route have been studied. X-ray diffraction study revealed that all the samples are in the orthorhombic symmetry with space group $A21am$. The dielectric study as a function of temperature demonstrated a ferroelectric to paraelectric transition is of diffuse type. The transition temperature (T_c) was found to be increased from 420 °C ($x = 0$) for BNBT to 500 °C ($x = 0.40$) at 500 MHz, thus broadening the utilization temperature range of the ceramics. Sample $x = 0.40$ with the lowest $TK\varepsilon$ value, indicating the best dielectric temperature stability in all samples. The very high oxygen vacancy of the sample $x = 0.40$ partially contributes to its higher T_c. However, $x = 0.10$ sample shows the lowest tan δ at 300 °C, which shows the lowest electrical conductivity in all the samples. The effect of Nd additives on the degree of diffuseness of the dielectric constant curves of BNBT was discussed by using modified Curie–Weiss law. The ferroelectric nature of the samples has been confirmed from the measurement of the hysteresis loop at room temperature.

1 Introduction

Bismuth layered structured ferroelectrics (BLSF) have been widely investigated for their high dielectric constant, diffuse phase transition, giant electrostriction, and relaxor ferroelectric properties that are useful for application in piezoelectric transducers, sensors, ferroelectric non-volatile memories (Fe-RAM), etc. [1]. Polycrystalline $BaBi_4Ti_4O_{15}$ (BBT) lies under the four-layered perovskite structure having Ba^{2+} (Barium) and Bi^{3+} (bismuth) ions at site-A and Ti^{4+} (titanium) ions at the site-B of its each orthorhombic perovskite block. The crystal chemistry associated with the origin of the ferroelectric behavior and dielectric phase transition in $MBi_4Ti_4O_{15}$ of BLSFs and they found that the size of M cation and the number of perovskites units in these compounds play a major role in the change in phase transition temperature (T_c) [2, 3]. This exhibits that the dielectric behaves like a relaxor with appreciable piezoelectric

Address correspondence to E-mail: sharmajp.rcr@gmail.com

https://doi.org/10.1007/s10854-021-05826-5

and ferroelectric characteristics. However, BBT ceramics are affected by problems linked with high dielectric loss, high conductivity, and increased dielectric dispersion with frequency [4, 5]. BLSFs attracted remarkable attention in the last years for application in non-volatile random access memory and high-temperature piezoelectric devices. The barium bismuth titanate (BBT) ceramics modified with La [6, 7], Nb [8], Ce [9], Sm [10], or with an excess of Bi_2O_3 [5, 11], have shown frequency-dependent relaxor behaviors. These materials present quite different dielectric constant values under the same measurement conditions. There have been few studies bent on improving the ferroelectric and/or dielectric properties with the addition of rare-earth (RE^{3+}) ions at the Bi^{3+} site in BBT; however, the results are accompanied by the reduction in transition temperature (T_c) [7, 12–15]. Since the BLSFs are best known for their high transition temperature, they are suitable for application in high-temperature piezoelectric transducers. A small enhancement in the electrical properties at the expense of reducing the T_c is unacceptable. The compositional fluctuations due to A/B site substitution and oxygen/bismuth vacancies affecting the electrical properties demand further understanding and investigation. The motivation is to enhance the ferroelectric and dielectric properties of BBT without affecting its T_c. The oxygen vacancies can be controlled by substituting RE^{3+} ions at the appropriate lattice site and optimum concentration. The substitution of trivalent RE^{3+} for Ba^{2+} causes a charge imbalance which is compensated by the formation of A-site cationic vacancies [6]. Also the stronger Re–O bond than the Bi–O and Ba–O bonds would restrain the movement of oxygen vacancies.

With these considerations in mind, Nd-doped BBT ceramics are prepared and studied concerning their structure, dielectric, and ferroelectric properties for the first time.

2 Experimental procedure

$Ba_{1-(3/2)x}Nd_xBi_4Ti_4O_{15}$ (BNBT) ceramics with different Nd concentrations (x = 0, 0.10, 0.20, 0.25, 0.30, and 0.40) are prepared using the solid-state reaction process. Stoichiometric quantity of carbonate and oxides with high purity, Nd_2O_3 (99.9%, Himedia Lab., India), Bi_2O_3 (99%, CDH, India Ltd.), and $BaCO_3$ & TiO_2 (purity ≥ 99%, Merck, India Ltd.), is hand grounded in an agate mortar to procure a uniform mixture by adding acetone and distilled water. Further 3 wt% of Bi_2O_3 was added to the initial stoichiometric ratio to balance the bismuth loss due to high-temperature processing. The obtained mixtures were calcined for 6 h at 900 °C. The calcined samples were ball milled for 4 h in the planetary ball mill (FRITSCH "Pulverisette 5"). The final milled powders were re-calcined for 12 h at 950 °C. The resultant powders were mixed with PVA and then pelletized at 60 kg/cm^2 employing a die of 5 mm radius. All pellets were sintered at 1000 °C for 12 h in a box furnace. The X-ray diffraction (XRD) technique was employed for structural investigation by using Cu-K_α radiation (Bruker D-8 Advanced, Germany). The XRD profile of each ceramics was recorded at 1°/min of scanning rate from 20° to 70° with a step size of 0.02°. The surface morphology and microstructural study of the sintered pellets were analyzed via a scanning electron microscope (SEM, JSM-6390, Japan). The dielectric behaviors as a function of the temperature of the pellets were measured by an LCR meter (IM3536, Hioki, Japan) from 30 to 500 °C. The Ferroelectric behavior (P–E loops) of BNBT samples was investigated by using a ferroelectric loop tracer at room temperature (Precision premier-II, Radiant, USA).

3 Results and discussion

3.1 XRD and microstructural analysis

X-ray diffraction spectra of BNBT powders show an orthorhombic structure with the space group $A21am$ as presented in Fig. 1 [4, 16]. The diffraction peak indexed as (1 1 9) plane shows the maximum intensity, indicating that all the compositions have pure bismuth layer perovskite with n = 4 (where n is the no. of perovskite layers) and well in accord with the available literature [17]. All samples show a single-phase character with no impurity peaks associated with the reactant oxides as observed in Fig. 1. The lattice parameters derived by using a standard CCP-14 program chekcell are listed in Table 1. There is no appreciable change in the lattice parameters observed for the samples with different Nd^{3+} concentrations. Although it is expected that the lattice constant could decrease due to the substitution of low radii Nd^{3+} (1.27 Å) in place of larger radii Ba^{2+} (1.61 Å) ion, the

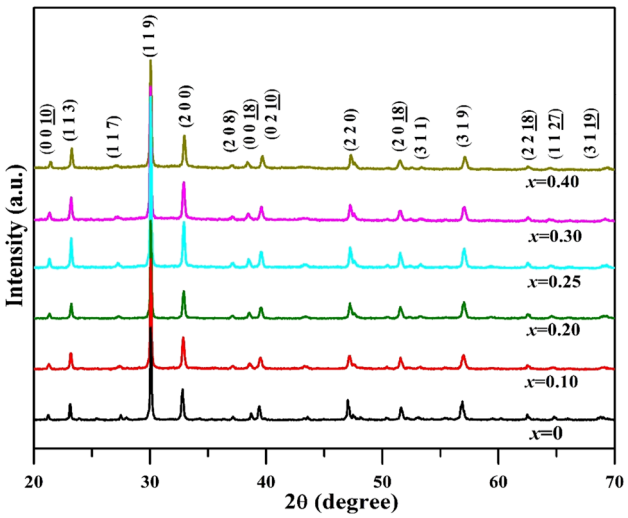

Fig. 1 X-ray diffraction patterns of the $Ba_{1-(3/2)x}Nd_xBi_4Ti_4O_{15}$ ceramics calcined at 950 °C for 12 h

Bi_2O_2 interlayer would act as a structural restriction that may not allow the unit cell volume/lattice constants to vary significantly [12]. Figure 2 shows the surface morphology of the pellets for all the compositions under study characterized by SEM. The pure BBT composition consists of mixed plate-like and spike-like grains that are irregularly shaped. However, for $x = 0.10$ composition, the grain morphology shows circular disk-shaped grains of size ~ 2 μm which is unique among all the samples. The disk-shaped plate-like grains are a characteristic component of bismuth layered compounds [18] that deformed with the increase in doping concentration. A very dense morphology is seen up to $x = 0.25$ after which porosity increases due to the lower diffusivity of Nd^{3+} ions that restrain the grain growth [19, 20]. The grain size (average) of the perovskite decreases with increasing the doping concentration.

3.2 Dielectric study

Figure 3 displays the temperature-dependent dielectric constant at different frequencies for the compositions with x = 0–0.40. The dielectric constant (ε') exhibits a broad inconsistency around 417 °C for the parent composition which is in agreement with the earlier studies [21, 22]. Small frequency dependence of dielectric dispersion around the temperature of dielectric maximum (T_m) is noticed for the BNBT (x = 0 and 0.10), along with the reduction in the peak dielectric constant (ε_m) with rise in frequency. This behavior is attributed to the diffused phase transition (ferroelectric–paraelectric) due to the change in structural symmetry at this temperature. However, T_m is frequency independent for higher Nd^{3+} concentration ($x > 0.10$). The diffuseness or broadness of the phase transition is found higher for the Nd^{3+} substituted samples as compared to pure BBT. The structural inhomogeneity or random disorderliness induced in the lattice due to smaller Nd^{3+} ion substitution on the Ba^{2+} site is the possible reason for the increase in diffuseness of the dielectric peaks. In comparison to reports suggesting typical relaxor behavior of BBT ceramics where the dielectric spectra merge completely (10 kHz to 1 MHz) for temperatures ($T > T_m$) [7, 23], the dielectric peaks for $x \leq 0.20$ samples almost merged at frequencies (> 100 kHz), indicating a signature to relaxor characteristics. The dielectric permittivity for a relaxor type ferroelectric obeys the modified Curie–Weiss law that defines the diffuseness of phase transition at elevated temperatures which is given by

$$\frac{1}{\varepsilon} - \frac{1}{\varepsilon_m} = \frac{(T - T_m)^{\gamma}}{C'} \quad (1)$$

Table 1 Variation in the lattice parameters, unit cell volume, phase transition temperature (T_c), remanent polarization P_r, coercive field E_c of $Ba_{1-(3/2)x}Nd_xBi_4Ti_4O_{15}$

Concentration (x)	a (Å)	b (Å)	c (Å)	Cell volume (Å^3)	T_c (°C)	P_r (μC/cm^2)	E_c (kV/cm)
$x = 0.0$	5.46 (13)	5.45 (14)	41.83 (72)	1245.57	420	0.71	18.01
$x = 0.10$	5.47 (64)	5.44 (72)	41.84 (51)	1248.28	432	0.29	16.43
$x = 0.20$	5.47 (33)	5.44 (34)	41.99 (81)	1251.26	456	0.23	15.48
$x = 0.25$	5.46 (71)	5.44 (23)	41.69 (53)	1240.58	476	0.11	10.40
$x = 0.30$	5.48 (42)	5.44 (35)	41.75 (74)	1246.59	492	0.44	16.91
$x = 0.40$	5.47 (51)	5.46 (01)	41.93 (20)	1253.54	500	0.58	22.10

Figures inside parentheses represents error value

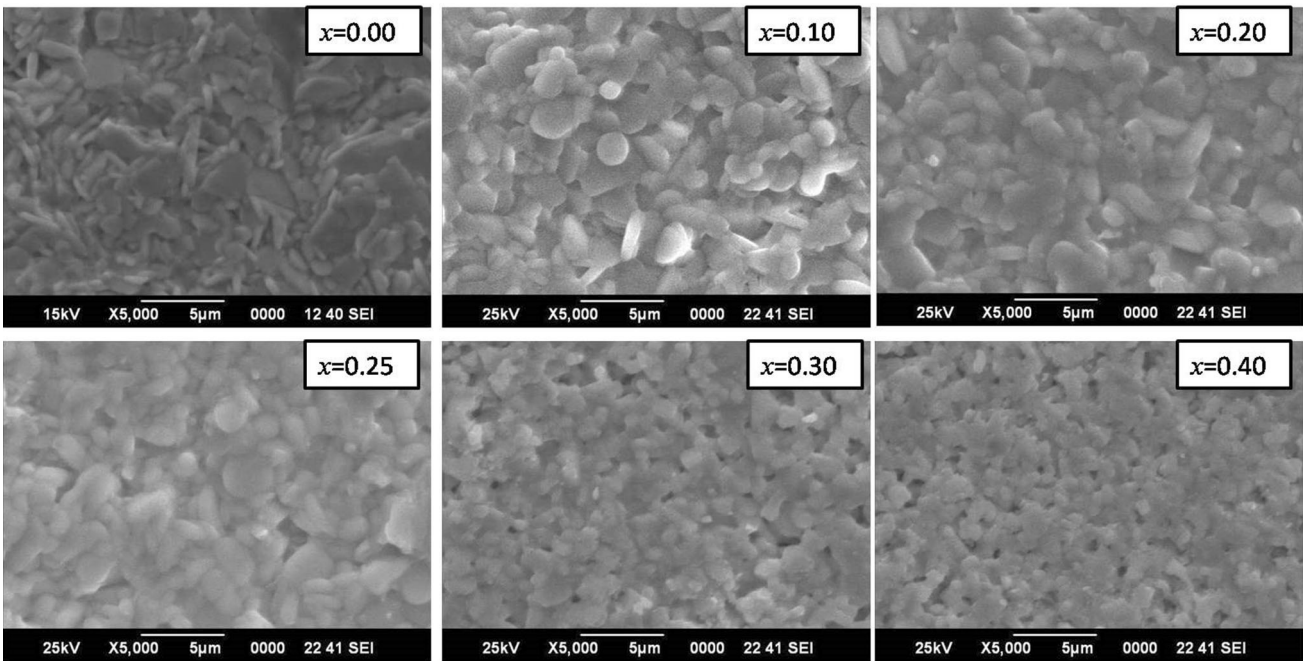

Fig. 2 SEM micrographs of sintered $Ba_{1-(3/2)x}Nd_xBi_4Ti_4O_{15}$ ceramics

where γ and C' (= $2\varepsilon_m\delta^2$) are constants [24]. The phase transition nature determines by γ; for a normal ferroelectric, the equation reduces to the Curie–Weiss law for $\gamma = 1$, while $\gamma = 2$ represents a relaxor material. The values of γ (diffusivity) and δ (diffuseness) are obtained by slope and intercept of the linear fit of $\ln(1/\varepsilon - 1/\varepsilon_m)$ vs. $\ln(T - T_m)$ for 500 kHz given in Fig. 4. The value of γ = 1.71 and δ = 15.63 for composition x = 0 enhanced to γ = 1.98 and δ = 16.95 for x = 0.25 composition, suggesting an increase in diffuseness or broadness of the dielectric peaks with the addition of neodymium [25]. Further, for x = 0.40 composition the value of γ and δ decreases to 1.40 and 13.65, respectively, due to the lower diffusivity of Nd^{3+} ions or an increase in porosity. It can be assumed that the increase in amount of Nd^{3+} concentration ($x > 0.25$) leads to compositional fluctuation [26] that helps stabilize perovskite phase in BBT [27].

Figure 5a shows the dielectric constant (temperature-dependent) and Fig. 5b dielectric loss for all the compositions at 500 kHz, respectively. A considerable increase in T_c is observed with an increase in Nd^{3+} ion concentration. Thus, extending the utilization temperature range of the ceramics. The structural inhomogeneity (distortion) arising due to the substitution of Nd^{3+} (1.27 Å) in place of higher ionic radii Ba^{2+} (1.61 Å) site results in a rise in T_m. However, the dielectric constant (ε') decreases with the rise in doping concentration, which may be attributed to the cationic vacancies created in the lattice that weakens the coupling of octahedral in the perovskites units. The substitution of trivalent Nd^{3+} for Ba^{2+} causes a charge imbalance which is compensated by the formation of A-site cationic vacancies. The oxygen vacancy will become the released centers of the internal stresses induced by ferroelectric phase transition with cooling temperature and then weakens the effect of internal stress on T_c and hence weakens the coupling of octahedral in the perovskites units [28]. Again, it is clear from Fig. 5b that the dielectric loss for Nd^{3+} composition is less than the undoped BBT, especially at high temperatures. The dielectric loss (ε'') in Aurivillius phases is affected by oxide ion conductivity or oxygen vacancies at elevated temperatures [29]. Here, the substitution of Nd^{3+} ion replacing Ba^{2+} compensates the oxygen vacancies in the lattice as per the defect chemistry reaction given in Eq. (1), i.e.,

$$Nd_2O_3 \rightarrow 2Nd_{Ba}^{\cdot} + 3O_o^x + V_{Ba}^{''}, \quad (2)$$

where O_o^x corresponds to an oxygen ion with a neutral charge at the oxygen site. Hence, the dielectric loss reduces with the stabilization of oxygen vacancies due to Nd^{3+} doping.

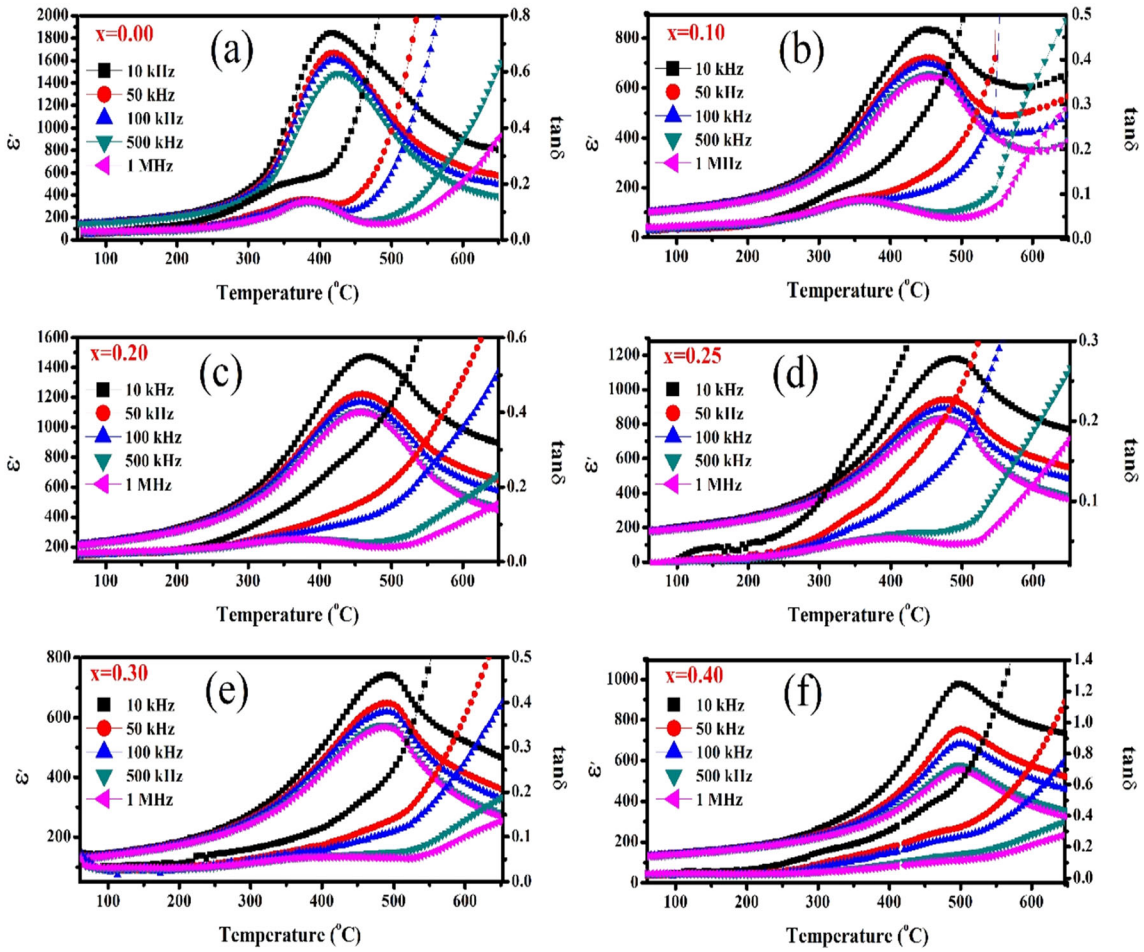

Fig. 3 Temperature-dependent dielectric constant and dielectric loss of $Ba_{1-(3/2)x}Nd_xBi_4Ti_4O_{15}$ (x = 0, 0.10, 0.20, 0.25, 0.30, and 0.40) ceramics at different frequencies

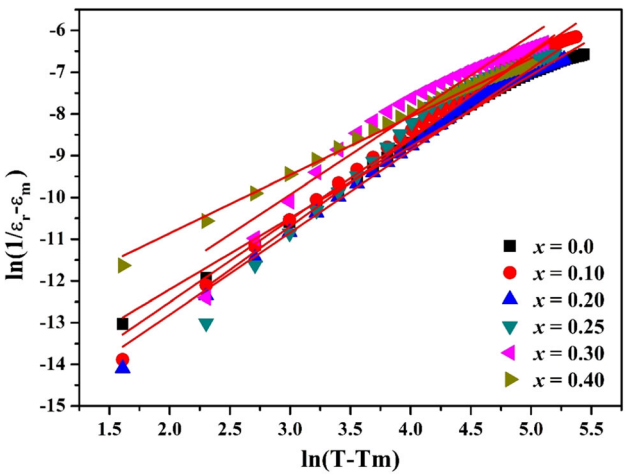

Fig. 4 Plots of $\ln(1/\varepsilon - 1/\varepsilon_m)$ as a function of $\ln(T - T_m)$ at 500 kHz for BNBT ceramics.

In order to further explore the dielectric temperature dependence of Nd-doped BBT ceramics, the temperature coefficient of dielectric constant ($TK\varepsilon$) as a function of temperature is shown in Fig. 5c. All the ceramics show good temperature stability up to 300 °C. Especially sample x = 0.40 has the lowest $TK\varepsilon$ value, indicating its best dielectric temperature stability among all the samples [28].

Figure 5d shows the dielectric loss (tan δ) of ceramics as a function of temperature (at 500 Hz). It is obvious that the tan δ of all the ceramics is less than 1 % below 300 °C. But the tan δ of the sample x = 0.40 begins to increase sharply at ~ 300 °C. It is known that the oxygen vacancy generated by the volatilization of Bi_2O_2 in BLSF will begin to move at a higher temperature which leads to the electric conduction of ceramics with sharp increasing tan δ. Therefore, x = 0.40 sample may involve much oxygen vacancy. So the much oxygen vacancy of x = 0.40 sample partly contributes to its higher T_c. However, x = 0.10 sample

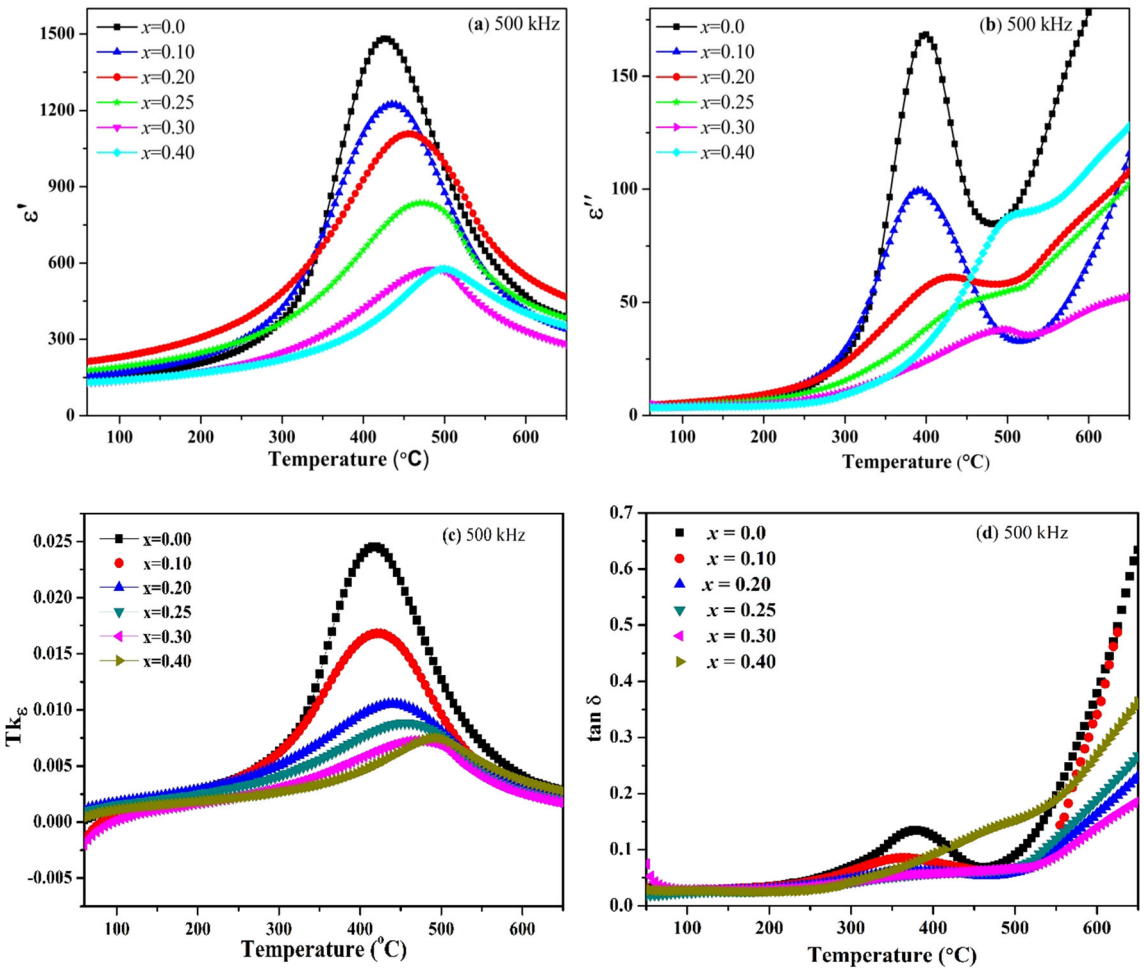

Fig. 5 **a** Temperature-dependent dielectric constant, **b** dielectric loss, **c** temperature stability of dielectric constant, and **d** tan δ of $Ba_{1-(3/2)x}Nd_xBi_4Ti_4O_{15}$ (x = 0, 0.10, 0.20, 0.25, 0.30, and 0.40) ceramics at 500 kHz

shows the lowest tan δ at 300 °C, indicating its lowest electric conductivity among all the samples [28, 30].

3.3 Ferroelectric study

Figure 6 illustrates the hysteresis (P–E) loops of the BNBT ceramics sample obtained by applying an electric field of about 60 kV/cm (maximum). The coercive field (E_c) and remanent polarization (P_r) values for different compositions are mentioned in Table 1. There is a decrease in P_r value from 0.71 to 0.11 μC/cm^2 (up to x = 0.20) and further increases to 0.58 μC/cm^2 (up to x = 0.40) composition. Similar behavior in E_c is also observed where it first reduces for composition with x = 0–0.20 and then increases beyond x = 0.20. There are several effects on remanent polarization. One of the possibilities here is the grain size of Nd-doped BBT samples that decreases with the increase in the doping level. The small grain size prevents the creation of large domains (ferroelectric) that decreases the efficient contribution to total polarization [31]. On the other hand, reports suggest that the perovskites with diffused dielectric phase transition character show less remanent polarization because of the coexistence of ferroelectric and paraelectric phases from room temperature to T_c [32]. As it is mentioned above that the diffuseness of dielectric peaks increases with Nd^{3+} substitution, this character may decrease the P_r values. Secondly, the quantity E_c reduces with the rise in neodymium concentration in doped BBT ceramics. The result may be ascribed to the reduction in the concentration of oxygen vacancy ($V_{\ddot{O}}$) as per the defect chemistry reaction given in Eq. 2. By screening/neutralizing the polarization charge, $V_{\ddot{O}}$ may influence the kinetics of the domain wall, or in other words, domain wall

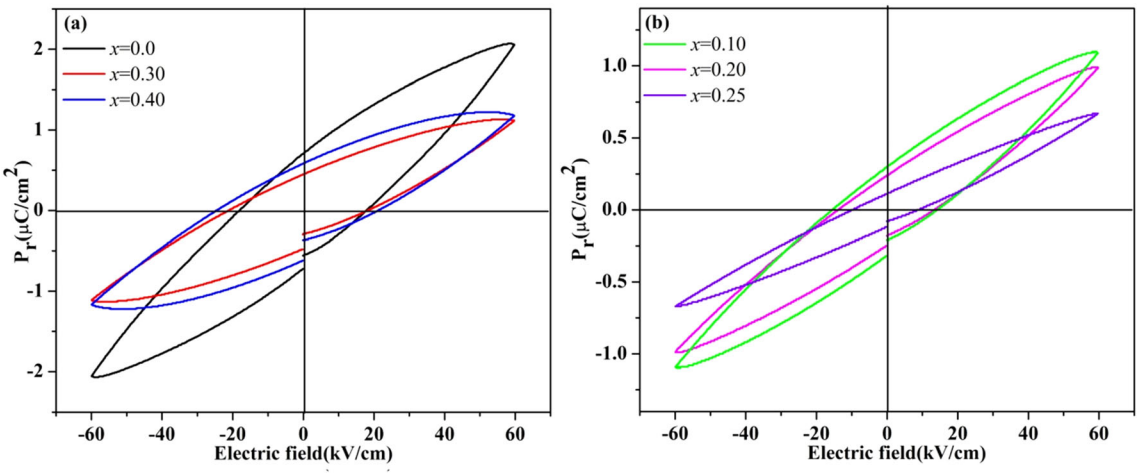

Fig. 6 Ferroelectric hysteresis loops recorded at room temperature under a maximum applied field of 60 kV/cm for **a** x = 0.0, 0.30, 0.40 and **b** x = 0.10, 0.20, 0.25

pinning (head-to-head polarization) might also stabilize the domain arrangement or configuration. Here the domain wall pinning reduces due to the stabilization of $V_{\ddot{O}}$ with the substitution of Nd^{3+} ion in place of Ba^{2+} ion. This indicates that the domain wall moves freely (disappear), which leads to the lowering of the E_c. Again the P_r and E_c values increase simultaneously for $x \geq 0.20$ BNBT series. The trivalent Nd^{3+} (1.27 Å) ions are prone to be substituted at the Bi^{3+} site (1.17 Å) since the difference in their ionic radii is smaller than Ba^{2+} (1.61 Å) ion. Moreover, the structure determination studies of BBT [4, 33] claimed the Ba ions randomly occupying Bi sites and/or entering the Bi_2O_2 layer. So there is a high chance of Nd ions being partially substituted at the Bi site with a higher doping level. This weakens defect mobility that contributes to domain pinning, thereby increasing polarization effects [34]. The bismuth vacancies formed due to partial substitution of Nd^{3+} ions may contribute to the accumulation of $V_{\ddot{O}}$ at domain walls, leading to an increase in the coercive field.

4 Conclusion

In summary, the ferroelectric $Ba_{1-(3/2)x}Nd_xBi_4Ti_4O_{15}$ ceramic samples have been prepared successfully via the solid-state reaction process. X-ray diffraction analysis confirmed the orthorhombic structure of the samples with the $A21am$ space group at room temperature. Ferroelectric to paraelectric transition has been observed from the dielectric properties as a function of temperature. The Nd^{3+} substitution on the Ba^{2+} site resulted in pronounced structural distortion and lattice mismatch, which leads to higher Curie temperature (T_c). It can be concluded that Nd^{3+} substitution enhances the utilization temperature range of the BBT ceramics. The $TK\varepsilon$ value of the sample enables us to find the best dielectric temperature stability in all samples, whereas the value of tan δ allows us to know the electrical conductivity in all the samples. The room-temperature hysteresis profile (P–E loop) validates the ferroelectric nature of the ceramics. A simultaneous change in P_r and E_c values were observed with the doping concentration. Although the low coercive field and high remanent polarization of material are best suitable for ferroelectric applications, there is no significant improvement in the P_r values as compared to pure BBT. However, a relatively low E_c is observed for x = 0.20 composition which can be processed further with better sintering conditions to control the grain growth for enhancing the P_r values.

Acknowledgement

The authors thank the University Department of Physics, Dr. Shyama Prasad Mukherjee University, Ranchi, for providing the necessary infrastructure to carry out our research.

Funding

Not applicable.

Data availability

Yes.

Declarations

Conflict of interest All the authors declare that they have no known competing interests or personal relationships that could have appeared to influence the work reported in this paper.

References

1. B.H. Park, B.S. Kang, S.D. Bu, T.W. Noh, J. Lee, W. Jo, Nature **401**, 682 (1999). https://doi.org/10.1038/44352
2. E.C. Subbarao, Integr. Ferroelectr. **12**, 33 (1996). https://doi.org/10.1080/10584589608225746
3. R.E. Newnham, R.W. Wolfe, J.F. Dorrian, Mater. Res. Bull. **6**, 1029 (1971). https://doi.org/10.1016/0025-5408(71)90082-1
4. A. Khokhar, M.L.V. Mahesh, A.R. James, P.K. Goyal, K. Sreenivas, J. Alloys Compd. **581**, 150 (2013). https://doi.org/10.1016/j.jallcom.2013.07.040
5. A. Khokhar, P.K. Goyal, O.P. Thakur, K. Sreenivas, Ceram. Int. **41**, 4189 (2015). https://doi.org/10.1016/j.ceramint.2014.12.103
6. A. Khokhar, P.K. Goyal, O.P. Thakur, A.K. Shukla, K. Sreenivas, Mater. Chem. Phys. **152**, 13 (2015). https://doi.org/10.1016/j.matchemphys.2014.11.074
7. A. Chakrabarti, J. Bera, J. Alloys Compd. **505**, 668 (2010). https://doi.org/10.1016/j.jallcom.2010.06.105
8. J.D. Bobić, M.M. Vijatović Petrović, J. Banys, B.D. Stojanović, Mater. Res. Bull. **47**, 1874 (2012). https://doi.org/10.1016/j.materresbull.2012.04.069
9. C.L. Diao, J.B. Xu, H.W. Zheng, L. Fang, Y.Z. Gu, W.F. Zhang, Ceram. Int. **39**, 6991 (2013). https://doi.org/10.1016/j.ceramint.2013.02.036
10. P. Fang, P. Liu, Z. Xi, Phys. B Condens. Matter **468–469**, 34 (2015). https://doi.org/10.1016/j.physb.2015.03.033
11. P.M.V. Almeida, C.B. Gozzo, E.H.N.S. Thaines et al., Mater. Chem. Phys. **205**, 72 (2018). https://doi.org/10.1016/j.matchemphys.2017.10.069
12. S. Kumar, K.B.R. Varma, J. Phys. D Appl. Phys. (2009). https://doi.org/10.1088/0022-3727/42/7/075405
13. D. Peng, H. Zou, C. Xu, X. Wang, X. Yao, J. Alloys Compd. **552**, 463 (2013). https://doi.org/10.1016/j.jallcom.2012.10.194
14. P. Fang, H. Fan, J. Li, L. Chen, F. Liang, J. Alloys Compd. **497**, 416 (2010). https://doi.org/10.1016/j.jallcom.2010.03.092
15. C.W. Ahn, H.J. Lee, S.H. Kang et al., J. Electroceram. **21**, 847 (2007). https://doi.org/10.1007/s10832-007-9308-y
16. B.J. Kennedy, Y. Kubota, B.A. Hunter, A. Ismunandar, K. Kato, Solid State Commun. **126**, 653 (2003). https://doi.org/10.1016/s0038-1098(03)00332-6
17. T. Badapanda, R. Harichandan, T. Bheesma Kumar et al., J. Mater. Sci. Mater. Electron. **27**, 7211 (2016). https://doi.org/10.1007/s10854-016-4686-z
18. J.A. Horn, S.C. Zhang, U. Selvaraj, G.L. Messing, S. Trolier-McKinstry, J. Am. Ceram. Soc. **82**, 921 (1999). https://doi.org/10.1111/j.1151-2916.1999.tb01854.x
19. X. Chou, J. Zhai, H. Jiang, X. Yao, J. Appl. Phys. (2007). https://doi.org/10.1063/1.2799081
20. M. Reddyprakash, S.K. Rout, A. Satapathy, T.P. Sinha, S.M. Sariful, Ceram. Int. **42**, 8798 (2016). https://doi.org/10.1016/j.ceramint.2016.02.122
21. S.K. Rout, E. Sinha, A. Hussian et al., J. Appl. Phys. (2009). https://doi.org/10.1063/1.3068344
22. P. Fang, H. Fan, Z. Xi, W. Chen, Solid State Commun. **152**, 979 (2012). https://doi.org/10.1016/j.ssc.2012.03.007
23. J.D. Bobić, M.M. Vijatović Petrović, J. Banys, B.D. Stojanović, Ceram. Int. **39**, 8049 (2013). https://doi.org/10.1016/j.ceramint.2013.03.075
24. K. Uchino, S. Nomura, Ferroelectrics **44**, 55 (1982). https://doi.org/10.1080/00150198208260644
25. C.L. Diao, H.W. Zheng, Y.Z. Gu, W.F. Zhang, L. Fang, Ceram. Int. **40**, 5765 (2014). https://doi.org/10.1016/j.ceramint.2013.11.015
26. Y. Chen, H. Zhou, S. Wang, Q. Chen, Q. Wang, J. Zhu, J. Alloys Compd. (2021). https://doi.org/10.1016/j.jallcom.2020.155500
27. W. Chaisan, R. Yimnirun, S. Ananta, D.P. Cann, Mater. Sci. Eng. B **132**, 300 (2006). https://doi.org/10.1016/j.mseb.2006.04.033
28. Y. Chen, D. Liang, Q. Wang, J. Zhu, J. Appl. Phys. (2014). https://doi.org/10.1063/1.4893366
29. K.R. Kendall, C. Navas, J.K. Thomas, H.C. zur Loye, Chem. Mater. **8**, 642 (1996). https://doi.org/10.1021/cm9503083
30. W.L. Liu, H.R. Xia, H. Han, X.Q. Wang, J. Crystal Growth **269**, 499 (2004). https://doi.org/10.1016/j.jcrysgro.2004.05.089
31. J. Zhai, X. Yao, J. Shen, L. Zhang, H. Chen, J. Phys. D Appl. Phys. **37**, 748 (2004). https://doi.org/10.1088/0022-3727/37/5/016

32. W. Cai, C. Fu, J. Gao, X. Deng, G. Chen, Z. Lin, Integr. Ferroelectr. **140**, 92 (2012). https://doi.org/10.1080/10584587.2012.741466
33. S. Kojima, R. Imaizumi, S. Hamazaki, M. Takashige, J. Mol. Struct. **348**, 37 (1995). https://doi.org/10.1016/0022-2860(95)08583-H
34. M. Ganguly, S.K. Rout, T.P. Sinha et al., J. Alloys Compd. **579**, 473 (2013). https://doi.org/10.1016/j.jallcom.2013.06.104